Microelectronics Reliability 50 (2010) 1973–1976

Contents lists available at ScienceDirect

Microelectronics Reliability

journal homepage: www.elsevier.com/locate/microrel

# Fabrication and enhanced field emission properties of novel silicon nanostructures

Srikanth Ravipati [a], Chang-Jung Kuo [b], Jiann Shieh [c,*], Cheng-Tung Chou [b], Fu-Hsiang Ko [a,**]

[a] Institute of Nanotechnology and Department of Materials Science and Engineering, National Chiao Tung University, Hsinchu 300, Taiwan
[b] Department of Chemical & Materials Engineering, National Central University, Hsinchu 300, Taiwan
[c] National Nano Device Laboratories, Hsinchu 300, Taiwan

ARTICLE INFO

*Article history:*
Received 6 December 2009
Received in revised form 20 May 2010
Available online 8 July 2010

ABSTRACT

We reported the fabrication and the field emission properties of two-tier novel silicon nanostructures. First, silicon nanopillars with ordered high aspect ratio were achieved by using conventional lithographic techniques to act as the field emission sources. Second, sharp-edged well-aligned silicon nanograss was fabricated on top of the nanopillars by means of hydrogen plasma dry etching to induce the field emission characteristics. The turn-on fields were obtained as 10.5 and 14.4 V/μm under current density of 0.01 mA/cm$^2$ for two-tier patterns separated by respective 5 μm and 2 μm spaces. The excellent field emission property from these novel nanostructures exhibited a great potential as high-performance field emitter arrays towards future nanoelectronic devices.



## 1. Introduction

Field emission is one of the main features of nanomaterials and nanostructures, and is of great commercial interest in displays and other electronic devices. Fowler and Nordheim developed a general model for electron emission from planar surfaces, and their model has been widely used for electron emission from large objects [1]. The main requirements for field emitters are low turn-on field, high current density, and good current stability. Recent advances in the fabrication of 1D nanostructures such as nanotubes [2,3], nanowires [4,5], and nanorods [6] have been considered to be good field-emission electron sources because of their high aspect ratios. Silicon nanostructures are of special interest due to their excellent field emission properties and process compatibility with Si technology. Several techniques have been employed to fabricate nanomasks, e.g., electron beam lithography [7], percolating of substrates before reactive ion etching [8,9], and ion bombardment with a heterogeneous material placing together with the object to be etched [10] etc. These processes are either expensive or suffered from lack of uniformity in terms of geometrical shape and distribution.

A one step approach like femtosecond laser processing [11] for micron sized sharp Si spikes and self masked dry etching [12] to produce silicon nanotips were also reported. Self-assembled silicon nanostructures and their field emission were also reported recently [13,14]. However, the field emission performance depends both on high aspect ratio and sharp tip of the nanostructures. The needle of tip shape of the nanowire drastically increases the aspect ratio and the field-enhancement factor [15], leading to a reduction in the turn-on field. This behavior has been related to localized states at the cap, space-charge effects, and adsorbents, but the reasons for this behavior are still unclear. Thus, field emission from 1-D materials requires further data in order to understand their field-emission mechanism. Here, we firstly report the fabrication of novel two-tier nanostructure (nanostructure on nanostructure) for the field emission application. Fig. 1 shows the schematic fabrication of Si nanograss on nanopillars. In the first step silicon 1.2 × 1.2 cm$^2$ nanopillars were fabricated by e-beam lithography and transformer-coupled plasma (TCP) etching system. In the second step hydrogen plasma etching was performed to fabricate well-aligned silicon nanograss on top of the nanopillars [16]. The turn-on fields are 10.5 and 14.4 V/μm at 0.01 mA/cm$^2$ for the two-tier patterns with nanopillars separated by 5 μm and 2 μm distance, respectively.

## 2. Experimental

The nanopillar patterns were defined through electron beam lithography (Leica WEPRINT 200) to have dimensions of 100 × 100 nm$^2$ and spacing of 2 and 5 μm. The depth of nearly 1 μm was etched using a transformer-coupled plasma system (Lam TCP 9400). The Si nanograss was prepared through hydrogen plasma etching in an inductively coupled plasma chemical vapor deposition (ICPCVD) system. The chamber was cleaned with $CF_4$ and $O_2$ plasma prior to performing the etching process; it was evacuated to a base pressure of 5 × 10$^{-5}$ torr with a substrate holder heated at 400 °C. After loading the boron doped 1–10 Ω cm *p*-type 6-in. (1 0 0) Si wafer, $H_2$ gas (160 sccm) was introduced and then the reactor pressure (30 mtorr) was maintained. The radio frequency (RF) power and bias power were 550 and

* Corresponding author. Tel.: +886 35726100x7716; fax: +886 35503814.
** Corresponding author. Tel.: +886 35712121x55803; fax: +886 35744689.
*E-mail address:* fhko@mail.nctu.edu.tw (F.-H. Ko).

0026-2714/$ - see front matter © 2010 Elsevier Ltd. All rights reserved.
doi:10.1016/j.microrel.2010.06.005

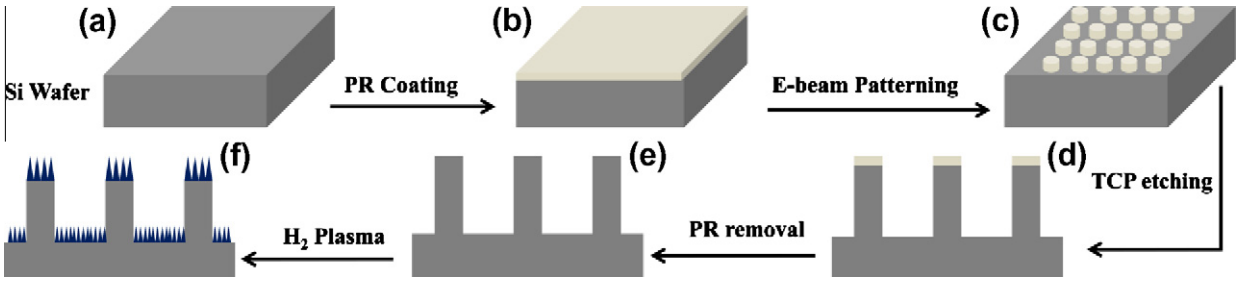


**Fig. 1.** Schematic of the silicon nanostructured fabrication steps: (a) ⟨1 0 0⟩ silicon wafer, (b) substrate after coating with photoresist, (c) E-beam patterning of photoresist with a diameter ~100 nm, (d) etching of silicon substrate in TCP chamber with a photoresist mask, (e) removal of photoresist with chemical etching, and (f) finally using hydrogen plasma to make the nanopillars sharp for field emitters.

280 W, respectively. The morphology and microstructure of silicon nanostructures were examined by scanning electron microscopy (SEM, JEOL JSM 6500F). Field emissions are characterized with a diode type configuration using a Keithley-237 high voltage semiconductor parameter analyzer. A schematic diagram of the experimental setup for two-electrode field emission is illustrated in Fig. 2. A diode Si/Al configuration with the as fabricated silicon nanostructures was used as the cathode and an ITO substrate as the anode, at a fixed separation of 60 μm. Field-emission measurements for the novel silicon nanostructures were performed in a high-vacuum chamber with a base pressure of about $8.0 \times 10^{-8}$ torr at room temperature. A direct-current voltage with a sweep step of 5 V was applied between the anode and cathode to establish an electric field. The emission current was measured with a Keithley-237 source-meter unit capable of providing up to 1100 V and 10 mA.

## 3. Results and discussion

SEM images of nanostructures are shown in Fig. 3a and b. These micrographs reveal a high density of well-aligned nanograss on the top of the nanopillar as well as the entire substrate. The nanograss exhibited a diameter ca. 20 nm with typical length of 200 nm after 30 min etching. Fig. 3c shows nanograss on both nanopillar and substrate and Fig. 3d shows sharp edged nanograss on nanopillar, which can enhance electron field emission from the emitter. The diameter of nanopillar is about 100 nm and the height is 1 μm. The average diameter and length of the blades of nanograss were approx. 20 and 200 nm, respectively – smaller than the typical dimensions of the nanograss in "black silicon" [17].

Fig. 4 shows a typical variation of the emission current density ($J$) with the electric field ($E$) measured at an anode-sample separation of 60 μm. The turn-on fields measured are 10.5 and 14.4 V/μm at 0.01 mA/cm$^2$ for two-tier patterns with nanopillars separated by 5 μm and 2 μm distance, respectively, and no turn-on fields were observed in nanograss and nanopillar samples alone.

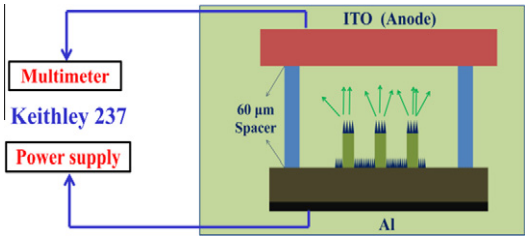


**Fig. 2.** Schematic diagram of the experimental setup for two-electrode field emission.

The field emission current–voltage characteristics can be expressed by a simplified Fowler–Nordheim (FN) [1] equation:

$$J = (A\beta^2 E^2/\Phi)\exp(-B\Phi^{3/2}/\beta E) \quad (1)$$

or

$$\ln(J/E^2) = \ln(A\beta^2/\Phi) - B\Phi^{3/2}/\beta E \quad (2)$$

where $J$ is the current density, $A$ and $B$ are constants ($A = 1.546 \times 10^{-6}$ AV$^{-2}$ eV, $B = 6.83 \times 10^3$ eV$^{-3/2}$ V μm$^{-1}$), $\Phi$ is the work function of the emitting material, which is 4.3 eV, $E$ is the electric field, and $\beta$ is the field-enhancement factor. For emitters following the Fowler–Nordheim (F–N) theory [1] in Eq. (1), the plot of $\ln(J/E^2)$ versus $1/E$ gives a straight line and its slope, $-(B\Phi^{1.5}/\beta)$, determines the surface local field-enhancement factor $\beta$ (also called the geometric enhancement factor). Fig. 5 showing the F–N plots at high bias voltages can be fitted well to the linear relationship which confirmed the measured data is truly from field emission.

Moreover, the FN slope in our current case can be written as

$$S = -6.83 \times 10^3 \Phi^{3/2}/\beta. \quad (3)$$

The field-enhancement factor $\beta$ may be used to demonstrate the degrees of field emission enhancement of tips of any shape on planar surfaces. Many researchers have demonstrated [18–20] that the field-enhancement factor $\beta$ is an important parameter of the emission properties; it depends on the geometry of the nanostructures, their crystal structure, and the distance between the emitter and anode. As the effective emission area and the work function for the samples are usually difficult to determine, $\beta$ can only be estimated from the slope of the fitting curve. Fig. 5 a and b are FN plot of two-tier nanostructure arrays, which fits well the linear relationship, as given by Eq. (2) and the slope $S$ of the linear part was obtained and, using the work function $\Phi$, the field-enhancement factor $\beta$ was calculated to be $1.62 \times 10^3$ and $1.32 \times 10^3$ for 5 μm and 2 μm distance samples respectively. This observation suggests the field-enhancement factors $\beta$ for both are nearly the same.

According to the Eqs. (1)–(3), the emission current ($I$) is strongly dependent on the following three factors [21]: (i) the work function of an emitter surface, (ii) the radius of curvature of the emitter apex and (iii) the emission area. In our present experiment the area (for calculating the current density, ($J$)) taken as $0.5 \times 0.5$ cm$^2$ with a hole in the cover slip for all the measurements. A variation in the emitter tip apex changes the magnitude of the field emission and excellent field emission performance was obtained for the two-tier nanostructures. The observed increase in field-enhancement factor $\beta$ of two-tier nanostructures can easily be understood as follows. The field-enhancement factor $\beta$ is generally related to emitter geometry and proportional to $h/r$, where $h$ is the height and $r$ is the curvature radius of an emitting center. As radius of curvature of the emitter apex decreases, the effective diameter of an

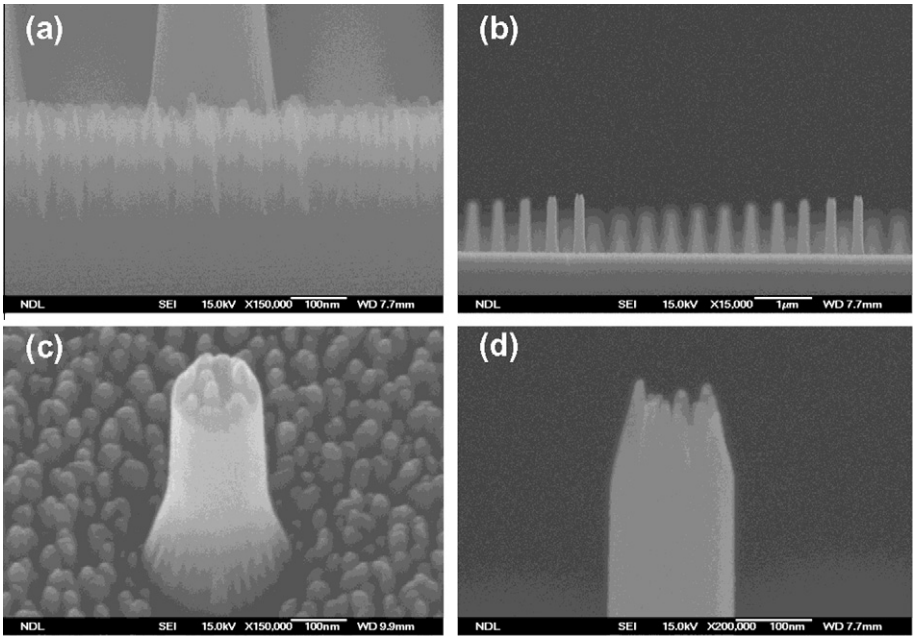


**Fig. 3.** SEM images of silicon nanostructures: (a) cross-sectional SEM image showing nanograss on Si wafer, (b) a side view of nanopillars separated by a distance 5 μm, (c) 30° tilt angle view of nanograss on nanopillar, and (d) cross-sectional image of emitter area.

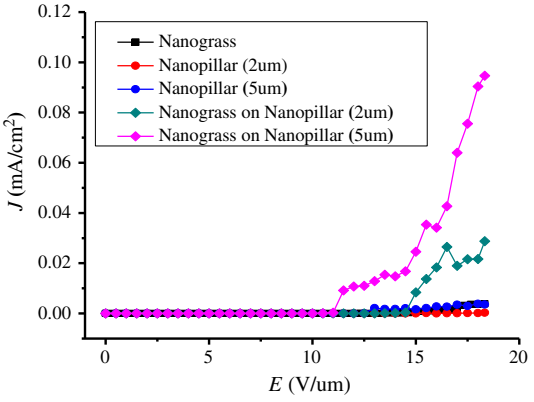


**Fig. 4.** Field emission current density–electric field ($J$–$E$) curves measured for nanostructures. The turn-on fields are 10.5 and 14.4 V/μm at 0.01 mA/cm$^2$ for two-tier patterns separated by 5 μm and 2 μm, respectively.

individual nanostructure and a curvature radius $r$ would decrease, resulting in an increase of $\beta$. Since it is the local electric field at the emission site that governs the emission, the distance between the nanostructures remains a crucial parameter to optimize the field emission. The low field emission performance of the two-tier nanostructures separated by a 2 μm distance apart are explainable by an electrostatic screening effect provoked by the proximity of neighboring nanostructures. As the density of nanostructures increases the charge per unit area increases and the charge reduces the potential drop perpendicular into the sample. The limit of zero distance between the nanostructures would correspond to a flat surface without field penetration. The sample of 2 μm spaced nanostructures is approaching to towards this limit with high density. Samples of two-tier nanostructures separated by a distance 5 μm are an optimum distance sufficient to reach substantial local fields with maximal emission current. Emission from the high density samples is poor because of reductions in the reductions in the field-enhancement factor due to screening effects. For the sample with low density there is an ideal compromise between the emitter

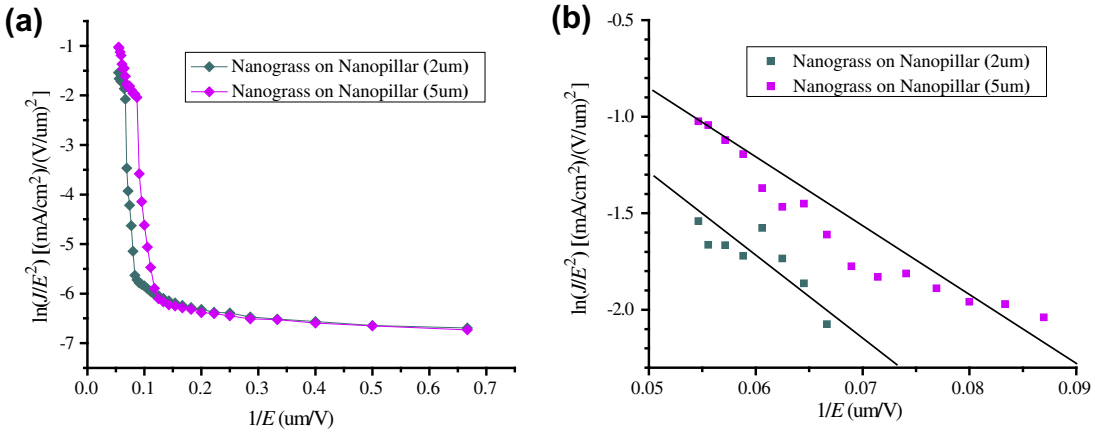


**Fig. 5.** ln($J/E^2$) versus $1/E$ from Fig. 4. For $1/E$ (a) between 0 and 0.67 and (b) between 0.054 and 0.09.

density and the inter distance of nanostructures, which is sufficiently large to avoid screening effects.

## 4. Conclusion

We have successfully developed a simple and an efficient method to fabricate the two-tier silicon nanostructures using the e-beam lithography in together with hydrogen plasma dry etching. The turn-on fields are estimated to be 10.5 and 14.4 V/μm at 0.01 mA/cm$^2$ for two-tier patterns with nanopillars separated by 5 μm and 2 μm respectively. The emission from high density nanostructures remains low because of screening effects between densely packed neighboring nanostructures; and the emission fields for low density nanostructures are high because the height and the distance between neighboring emitters are both sufficient to reach a high field-enhancement factor to avoid screening effects. The observation demonstrates a great potential toward high-performance field emitters for future nanoelectronic devices.

## Acknowledgements

This study was supported partially by the National Science Council of Taiwan (NSC 97-2221-E-492-002 and NSC 97-2120-M-009-007). We thank Yan-Chen Chen, Fu-Ju Hou, Hung-Min Chen and Chao-Chia Cheng for help in preparing these samples.

## References

[1] Fowler RH, Nordheim LW. Electron emission in intense electric fields. Proc Roy Soc Lond A 1928;119:173–81.
[2] De Heer WA, Châtelain A, Ugarte D. A carbon nanotube field-emission electron source. Science 1995;270:1179–80.
[3] Fan SS, Chapline MG, Franklin NR, Tombler TW, Cassell AM, Dai HJ. Self-oriented regular arrays of carbon nanotubes and their field emission properties. Science 1999;283:512–4.
[4] Wu ZS, Deng SZ, Xu NS, Chen J, Zhou J, Chen J. Needle-shaped silicon carbide nanowires: synthesis and field electron emission properties. Appl Phys Lett 2002;80:3829–31.
[5] Chen J, Deng SZ, Xu NS, Wang SH, Wen XG, Yang SH, et al. Field emission from crystalline copper sulphide nanowire arrays. Appl Phys Lett 2002;80:3620–2.
[6] Xi GC, Liu YK, Liu XY, Wang XQ, Qian YT. Mg-catalyzed autoclave synthesis of aligned silicon carbide nanostructures. J Phys Chem B 2006;110:14172–14178.
[7] Chen W, Ahmed H. Fabrication of high aspect ratio silicon pillars of <10 nm diameter. Appl Phys Lett 1993;63:1116–8.
[8] Seeger K, Palmer RE. Fabrication of silicon cones and pillars using rough metal films as plasma etching masks. Appl Phys Lett 1999;74:1627–9.
[9] Tomihari Y. US patent no. 2000 6057172.
[10] Yoshida H, Urushido T, Miyake H, Hiramatsu K. Formation of GaN self-organized nanotips by reactive ion etching. Jpn J Appl Phys 2001;40:L1301–4.
[11] Her TH, Finlay RJ, Wu C, Deliwal S, Mazur E. Microstructuring of silicon with femtosecond laser pulses. Appl Phys Lett 1998;73:1673–5.
[12] Hsu CH, Lo HC, Chen CF, Wu CT, Hwang JS, Das TsaiJ, et al. Generally applicable self-masked dry etching technique for nanotip array fabrication. Nano Lett 2004;4:471–5.
[13] Lu CT, Johnson S, Lansley SP, Blaikie RJ, Markwitz A. Atmospheric pressure operation of a field emission diode based on self-assembled silicon nanostructures. J Vac Sci Technol B 2005;23:1445–9.
[14] Bari MR, Blaikie RJ, Fang F, Markwitz A. Conductive atomic force microscopy study of self-assembled silicon nanostructures. J Vac Sci Technol B 2009;27:3051–4.
[15] Zhou J, Gong L, Deng SZ, Chen J, She JC, Xu NS, et al. Growth and field-emission property of tungsten oxide nanotip arrays. Appl Phys Lett 2005;87:223108–10.
[16] Shieh J, Lin CH, Yang MC. Plasma nanofabrications and antireflection applications. J Phys D Appl Phys 2007;40:2242–6.
[17] Dorrer C, Rühe J. Wetting of silicon nanograss: from superhydrophilic to superhydrophobic surfaces. Adv Mater 2008;20:159–63.
[18] Bonard JM, Dean KA, Coll BF, Klinke C. Field emission of individual carbon nanotubes in the scanning electron microscope. Phys Rev Lett 2002;89:197602–5.
[19] Rossi MC, Salvatori S, Ascarelli P, Cappelli E, Orlando S. Effect of nanostructure and back contact material on the field emission properties of carbon films. Diamond Relat Mater 2002;11:819–23.
[20] Au FCK, Wong KW, Tang YH, Zhang Bello I, Lee ST. Electron field emission from silicon nanowires. Appl Phys Lett 1999;75:1700–2.
[21] Xu NS, Huq SE. Novel cold cathode materials and applications. Mater Sci Eng R. 2005;48:47–189.